Journal of Physics:
Conference Series

PAPER • **OPEN ACCESS**

Comparison of Different Turbulence Models in Numerical Calculation of Low-Speed Flow around NACA0012 Airfoil

To cite this article: Zhaozheng Sun and Wenhui Yan 2023 *J. Phys.: Conf. Ser.* **2569** 012075

Comparison of Different Turbulence Models in Numerical Calculation of Low-Speed Flow around NACA0012 Airfoil

Zhaozheng Sun[1] and Wenhui Yan [1*]

[1] School of Mechanical and Materials Engineering, North China University of Technology, Beijing, 100144, China

EMAIL: sun.zhaozheng@foxmail.com (Zhaozheng Sun); abuaa@163.com(Wenhui Yan)

*Correspondence: abuaa@163.com(Wenhui Yan)

Abstract : To further develop a more effective turbulence model and improve the calculation accuracy of the flow, a new turbulence model was constructed using the deformation rate tensor, grouping the average. Due to the need to evaluate the applicability of the new turbulence model in the numerical calculation, the flow around the NACA0012 airfoil with a Mach number of 0.15 and multiple angles of attack was calculated on the OpenFOAM calculation platform based on grid independence research. The Spalart-Allmaras (S-A) model and the newly proposed turbulence model were adopted. The surface pressure and lift coefficients of the NACA0012 airfoil were calculated and compared with the experimental data. It was revealed that the two models simulated the flow around the airfoil well, and the S-A model was slightly better for calculating the airfoil pressure coefficient. The new turbulence model was more accurate for calculating the lift coefficient, thus illustrating the preliminary applicability of the new model to the low-speed flow around the airfoil.

1. Introduction

In recent years, with the dramatic increase in computer computing power, computational fluid dynamics has been widely applied in aerospace, automotive design, chemical design, etc., and numerical simulation techniques have also received attention from many countries worldwide. For example, the National Aeronautics and Space Administration (NASA) developed and released the "Computational Fluid Dynamics Vision 2030" planning document, and NASA reached a consensus with US government agencies to conduct research in six fields, including supersonic combustion and boundary layer flow mechanism [1-3]. Moreover, there are varying influencing factors such as geometric shape, mesh distribution, physical model, and numerical calculation method when the numerical simulation is carried out for more complex engineering projects. The numerical calculation method is of particular interest to scholars. Flow around the airfoil is one of the common problems in engineering practice, such as aircraft takeoff and landing, numerical simulation of multi-stage compressors and multi-stage turbines, etc. The study of airfoil boundary layer fluid is conducive to improving the control method of fluid flow and designing a better aerodynamic shape. Therefore, the study of flow around airfoils exhibits important engineering application value.

Based on the RANS method, Yan Wenhui et al. [4-5] applied the elliptical equation mesh method proposed by Hilgenstock to generate a structured mesh and numerically simulated NACA4412 airfoil.

The Gao-Yong turbulence model was more suitable for simulating the wake relaxation effect of flow around an airfoil. The unsteady time-averaged calculation results were superior to the steady calculation values. Qiu Fusheng et al. [6] numerically calculated the wing of a light sports aircraft based on the MDR turbulence model. They concluded that compared to the standard turbulence model, the κ-ε turbulence model with dissipation rate correction could better simulate the flow around an airfoil in the wake region. Yang Yuxiao et al. [7] simulated the cavitation of sheet clouds around the hydrofoil using static and adaptive mesh techniques and analyzed the causes of cavitation shedding. It was noted that the adaptive mesh could better balance the mesh resolution and computational complexity. The interaction of vortices and vacuoles formed on the upper surface behind the hydrofoil was very obvious. Based on the dynamic grid technique, Qian Yu et al. [8] investigated the dynamic stall of NACA0012 airfoil in unsteady flow. They demonstrated that dynamic mesh technology and the SST turbulence model could well capture the dynamic stall process of the airfoil through numerical calculations and comparison of experimental results. Based on the non-embedded PC (polynomial chaos) expansion method, Zhao Hui [9] et al. adopted the S-A model to simulate the RAE2822 transonic airfoil numerically and investigated the effect of the uncertainties of the nine parameters of the S-A turbulence model on the numerical simulations, and demonstrated that the established PC expansion could accurately illustrate the response of the output to the input by comparing the PC expansion with computational fluid dynamics (CFD) calculation. Based on the one-equation S-A model, two-equation Realizable model, and SST model in vortex viscosity model, Gu Running et al. [10] numerically simulated NACA0012 airfoil at different angles of attack and different Mach numbers and verified the accuracy of the three turbulence models for simulating high Mach number flow by comparing with wind tunnel experiments. Xue Yangliu et al. [11] applied the SDES method to numerically simulate the unsteady turbulent flow of a dynamic airfoil stall. They compared it with the DDES method and wind tunnel experimental results to provide a new RANS/LES method for numerical simulation of airfoil aerodynamics. ZHANG et al. [12] explored the low-speed flow around the S809 wing by combining the experimental data with numerical simulation and experimental observations. The improved data assimilation technique could accurately exhibit complex turbulence field problems such as wing flow.

This paper adopted the open-source software OpenFOAM to model the new model obtained by grouping the average turbulent fluctuation velocity. Additionally, the Spalart-Allmaras (S-A) model and the new model were applied to numerically calculate the low-speed flow around the NACA0012 airfoil, with the simulated angle of attack of 0-15° and the inflow Mach number of 0.15, the Reynolds number of 6×106 based on the airfoil chord length and inflow conditions, and the ambient temperature of 300 K. The eddy current changes on the upper and lower sides of the wing, especially at the trailing edge, could be observed under these conditions. This paper adopted two turbulence models to simulate the NACA0012 airfoil numerically, and the surface pressure coefficient, lift coefficient, eddy current field, and streamlined distribution of the airfoil were obtained. Besides, the applicability of the new turbulence model for the solution of the airfoil flow problem was also verified by comparing it with the experimental values in the literature [13].

2. Control Equations and Numerical Methods

2.1. Control equations and turbulence models

The control equation used in this paper was the Navier-Stokes (N-S) equations in Reynolds-averaged incompressible form, and the continuity equation and momentum equation in the rectangular coordinate system is in the following differential forms:

$$\frac{\partial \boldsymbol{u}_j}{\partial \boldsymbol{x}_j} = 0 \tag{1}$$

$$\frac{\partial(\boldsymbol{u}_i)}{\partial t} + \boldsymbol{u}_j \frac{\partial \boldsymbol{u}_i}{\partial \boldsymbol{x}_j} = -\frac{1}{\rho}\frac{\partial p}{\partial \boldsymbol{x}_i} + \frac{1}{\rho}\frac{\partial}{\partial \boldsymbol{x}_j}(\boldsymbol{\sigma}_{ij} + \boldsymbol{\sigma}_{ij}^{turb}) \tag{2}$$

Wherein, ρ represents density, p means pressure, $\boldsymbol{u}_i$ represents velocity, $\boldsymbol{\sigma}_{ij}$ represents laminar viscous stress, and $\boldsymbol{\sigma}_{ij}^{turb}$ indicates turbulent viscous stress. The new turbulence model in this paper was constructed based on the group average of turbulent fluctuation velocity. The instantaneous velocity of turbulence can be expressed as $\boldsymbol{u} = \overline{\boldsymbol{u}} + \boldsymbol{u}'$, where $\overline{\boldsymbol{u}}$ it means the average ensemble velocity and $\boldsymbol{u}'$ means the corresponding fluctuation velocity. Since the ensemble average of all fluctuation velocities at a point in space is 0, using the first-order fluctuation velocity $\boldsymbol{u}'$ in the turbulence modeling process is impossible, which is physically real and plays an important role. As a result, the positive and negative groups based on the mean value were grouped and weighted to obtain the mean information of the non-zero first-order fluctuation velocity, as described in the literature [14]. The specific turbulence model equations are illustrated below.

The fluctuation continuity equation is:

$$\frac{\partial \hat{\boldsymbol{u}}_j}{\partial \boldsymbol{x}_j} = 0 \tag{3}$$

The group average fluctuation velocity equation is:

$$\frac{\partial \hat{\boldsymbol{u}}_j}{\partial t} + \frac{\partial\left(\hat{\boldsymbol{u}}_j \boldsymbol{u}_i + \hat{\boldsymbol{u}}_i \boldsymbol{u}_j + \hat{p}\delta_{ij}\right)}{\partial \boldsymbol{x}_i} = \frac{1}{\rho}\frac{\partial\left(\hat{\boldsymbol{\sigma}}_{ij} + \hat{\boldsymbol{\sigma}}_{ij}^{Turb} - \boldsymbol{\sigma}_{ij} - \boldsymbol{\sigma}_{ij}^{Turb}\right)}{\partial \boldsymbol{x}_i} \tag{4}$$

Wherein $\hat{\boldsymbol{u}}_j$ represents the group average fluctuation velocity and $\hat{\boldsymbol{\sigma}}_{ij}$ the laminar stress corresponding to the fluctuation velocity after the group average, similar to the calculation $\boldsymbol{\sigma}_{ij}$ $\hat{\boldsymbol{\sigma}}_{ij}^{Turb}$. It means the turbulent stress corresponding to the fluctuation velocity after the group average, which is similar to the calculation of $\boldsymbol{\sigma}_{ij}^{turb}$, but only $\boldsymbol{u}_j$ is replaced with $\hat{\boldsymbol{u}}_j$.

In this paper, the turbulent viscosity coefficient is constructed in the form of the following:

$$\mu_T = \beta \frac{\rho \hat{u}_i \hat{u}_i}{2S} \tag{5}$$

Wherein, ρ represents the density, the coefficient β is 0.2-0.6, and S indicates the deformation rate tensor.

A detailed description of the S-A turbulence model is available in the literature [15].

2.2. Numerical methods, meshes, and boundary conditions

This paper adopted the OpenFOAM platform to model the new turbulence model. A simple foam solver using the finite volume method was used to solve the N-S equation of steady-state incompressible Newtonian fluid. The coupling of pressure and velocity was calculated *via* SIMPLE/SIMPLEC to ensure the accuracy and stability of the calculation.

In this paper, with NACA0012 airfoil flow as the research object, the S-A model and new turbulence model, after grouping the average turbulent fluctuation velocity, were applied to numerically simulate the flow around an airfoil at a low Mach number. The differences between the two turbulence models for simulating flow around an airfoil at a low Mach number were compared. The computational domain of the NACA0012 airfoil is shown in Figure 1, and the chord length (characteristic length) of a dimensionless airfoil is c = 1.0. Further, to reduce the influence of the far field on the calculation result, the outer boundary of the computational domain is about 500 c, away from each direction. As shown in Figures 2 and 3, the extruded C-type structured grid provided in the literature [16-17] is used as a computational grid in this paper to locally encrypt the front and tail edges of the airfoil. To verify the grid independence, three sets of grids with mesh numbers of 449×49, 897×257 and 1793×513were calculated, respectively, and it was found that the results of the other two sets of meshes were consistent except that the boundary layer of the first set of meshes was not encrypted sufficiently. The pressure coefficients (C_p) of the airfoil surface calculated using the S-A model on two sets of grids, 897 ×257 and 1793 × 513, shown in Figure 4, and it can be observed that

the results of these two sets of grids are coincident. This paper used the structured mesh of 897×257 for subsequent calculation, with the airfoil wall y^+<1.0.

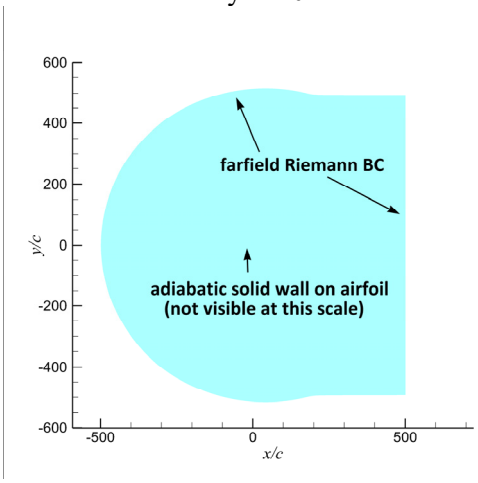

Figure 1: Computational domain of NACA0012 airfoil

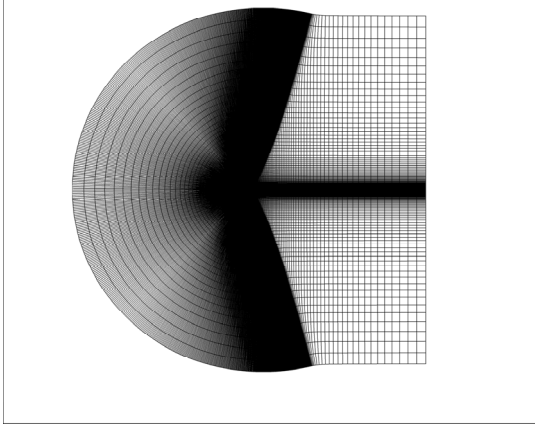

Figure 2: Computational domain grid

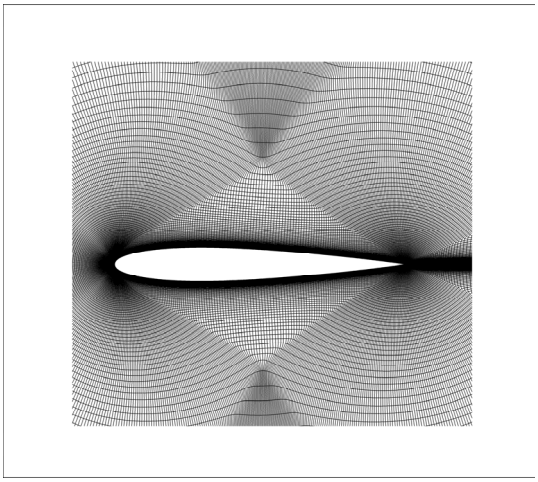

Figure 3: Computational grid near NACA0012 airfoil Figure

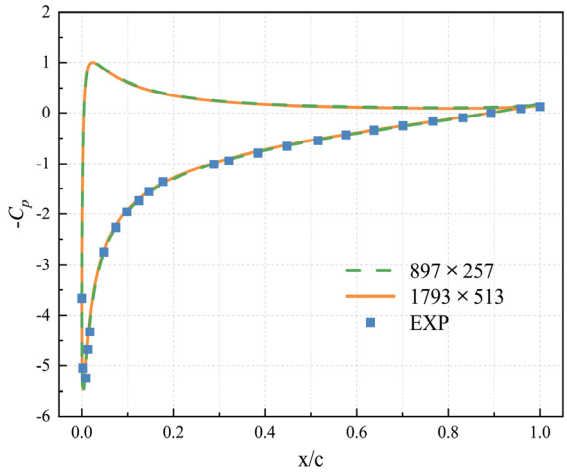

Figure 4: NACA0012 airfoil surface pressure coefficient

The boundary conditions are inlet boundary, outlet boundary, solid wall boundary, and empty boundary. As stated in Table 1, for the inlet and outlet boundaries of the computational domain, the free flow boundary condition was adopted, and the no-slip adiabatic condition was provided for the airfoil object surface boundary. The initial calculation field is the uniform flow field under incoming flow conditions.

Table 1 The boundary conditions used in OpenFOAM for the computational domain

	Airfoil	Inlet/outlet	Front and back
U	fixed-value	freestream velocity	empty
p	zero gradient	freestreamPressure	empty
nuTilda	fixed-value	freestream	empty
nut	nutLowReWallFunction	freestream	empty

3. Comparative Analysis of Calculated Results

The calculated airfoil surface pressure coefficient and the experimental values of the two turbulence models at angles of attack of 0°, 6.03°, 10°, and 15° are shown in Figures 5(a)-5(d) respectively (the experiment at 6.03° angle of attack was not performed in the literature [13]). The new turbulence model obtained after grouping the average turbulent fluctuation velocity and the S-A turbulence model could more accurately simulate the airfoil surface pressure coefficient. Still, there are differences between these two models in some aspects. The surface pressure number obtained using the new model at a small part of the trailing edge is larger than the experimental value, but the deviation is small. Besides, the S-A model can calculate the pressure coefficients on the airfoil surface better than the new turbulence model when the airfoil is close to the stall state with the gradual increase of the head angle.

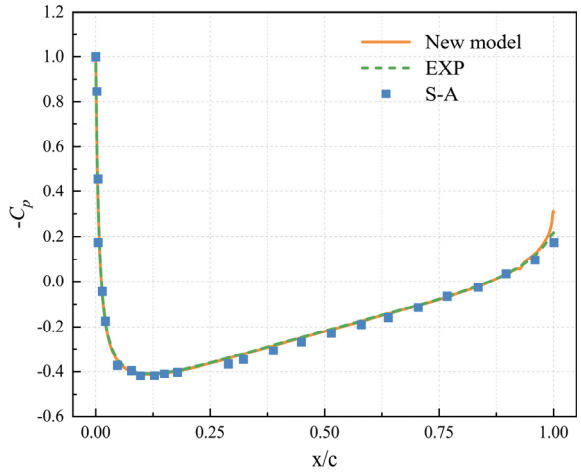

(a) 0° angle of attack

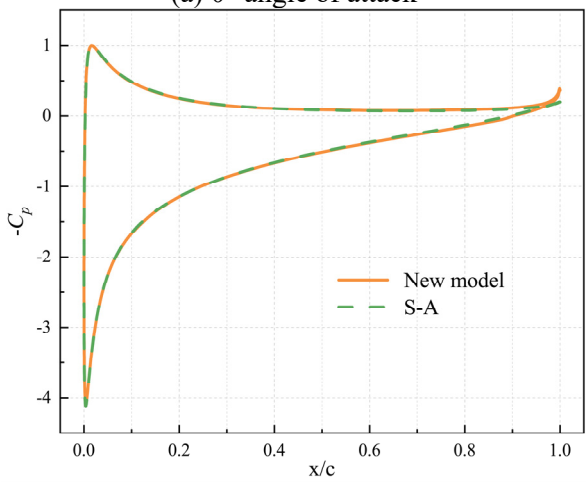

(b) 6.03° angle of attack

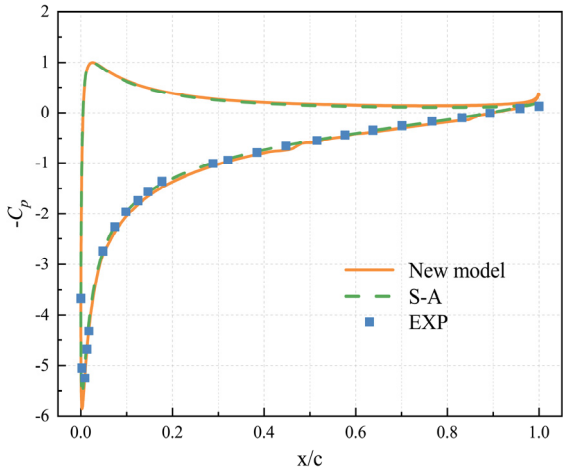

(c) 10° angle of attack

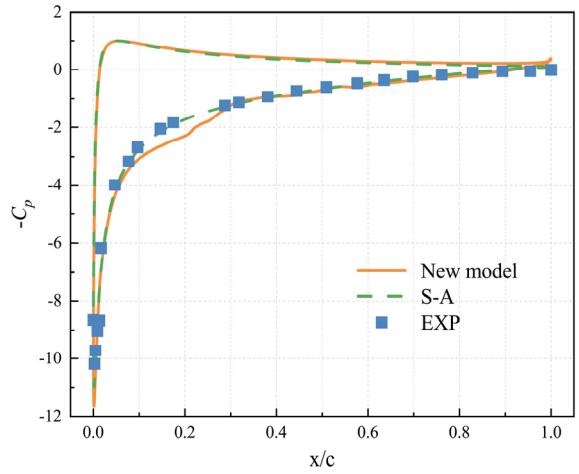

(d) 15° angle of attack

Figure 5: NACA0012 airfoil surface pressure coefficient at a different angle of attack

The vortex diagrams of the two models at different angles of attack are illustrated in Figure 6, and it can be seen that the diagrams that both models can better simulate the process of airfoil development from stable flow to dynamic stall with the increase of angle of attack. The laminar flow is attached to the surface of the airfoil at the angle of attack of 0°. From the figure, it can be observed that the new turbulence model is more stable than the S-A model. At the angle of attack of 15°, as shown in the figure, the vortex cloud diagram of the S-A model is more stable than that of the new turbulence model. Figures 7(a) and 7(b) are the streamlined diagrams of the two models at the NACA0012 airfoil at an attack angle of attack of 15°. The comparison revealed that the results obtained using the two turbulence models are consistent around the entire airfoil, indicating that the new turbulence model can better simulate the flow field at low speed.

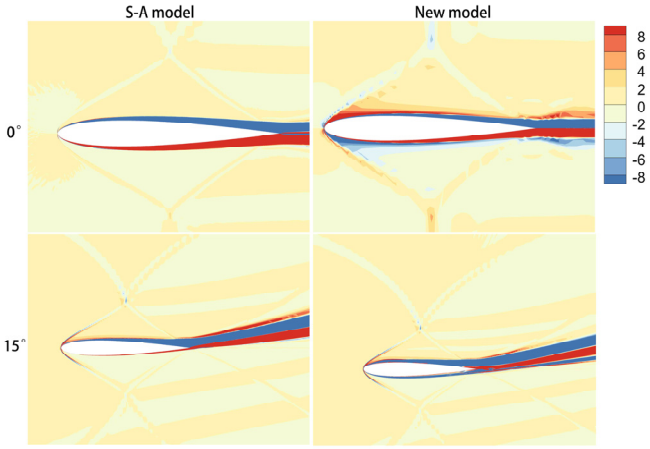

Figure 6: Vortex cloud diagram of NACA0012 airfoil

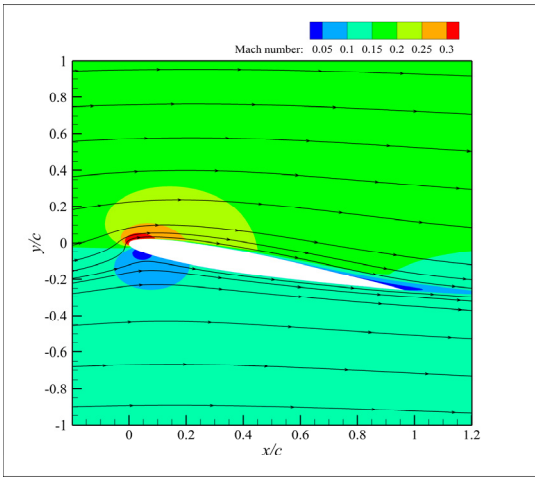

(a) Streamlines for S-A model calculation

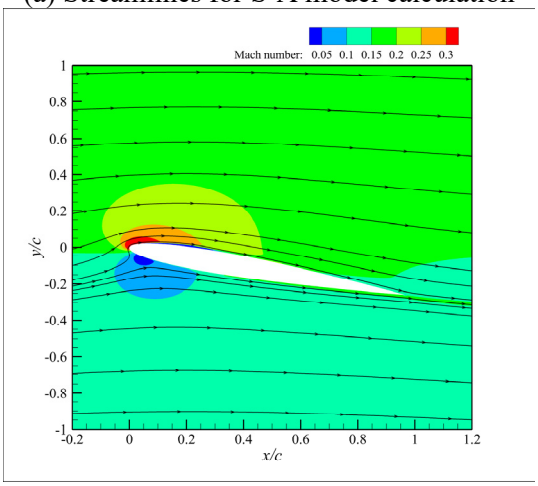

(b) Streamlines for new model calculation

Figure 7: Comparison of Streamline diagrams for the two turbulence model

The airfoil lift coefficients (C_L) calculated using two turbulence models are compared with the experimental data in Figure 8, and the abscissa α means the airfoil's angle of attack. According to the diagram, the lift coefficients calculated using the new and S-A turbulence models are consistent with the experimental data. At the angle of attack of more than 8 °, the lift coefficient calculated using the S-A model is significantly smaller than the experimental value, and the lift coefficient obtained using the new turbulence model is slightly larger than the experimental results. Still, it is more in line with the experimental value. At an angle of attack of less than 8 °, the lift coefficient calculated using the S-A model is more consistent with the experimental value. Still, the lift coefficient obtained by the new turbulence model is less different from the experimental value, which suggests that the new turbulence model possesses better prediction of airfoil lift characteristics.

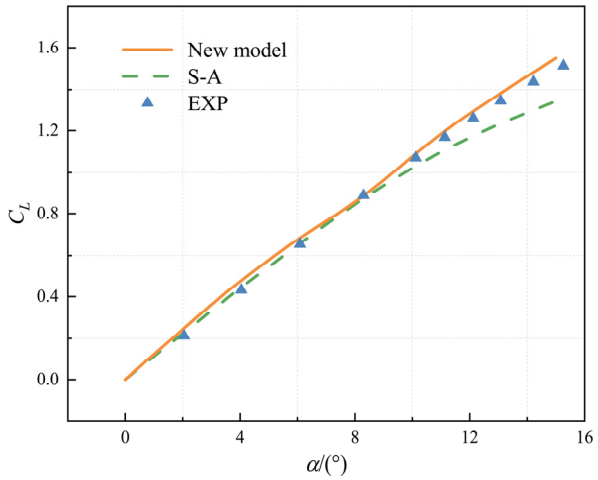

Figure 8: Lift coefficient of NACA0012 airfoil

4. Conclusions

This paper takes the low-speed flow of NACA0012 airfoil as the research object. Based on the OpenFOAM calculation platform, the new and S-A turbulence models obtained after grouping the average turbulent fluctuation velocity were adopted to simulate the flow numerically. Also, the airfoil's surface pressure coefficient and lift coefficient were compared. The following conclusions are obtained:

(1) Generally, the results calculated using both turbulence models agree with the experimental data and can meet the application requirements in engineering practice. For calculating the airfoil surface pressure coefficient, the S-A model is slightly better than the new turbulence model, especially at the airfoil trailing edge and a large angle of attack.

(2)The two turbulence models obtain similar calculation results for the vorticity of the flow field. Still, the S-A model is superior to the new turbulence model at a large angle of attack.

(3)The airfoil lift coefficients calculated using both the new turbulence model and the S-A model differ from the experimental values to some extent. Still, the results calculated using the new turbulence model are more accurate and closer to the experimental values, especially at the angle of attack of more than 8°. The new turbulence model possesses better prediction of airfoil lift characteristics.

References

[1] H. Y. Sun, Z. X. Sun, X. L. Chen, et al. A review of the progress of hypersonic numerical simulation in the United States, National Defense Science & Technology 43.10 (2022) 42–47. doi:10.13943/j.issn1671-4547.2022.04.08.

[2] J. D. Schmisseur. Hypersonics into the 21st century: A perspective on AFOSR-sponsored research in aerothermodynamics, Progress in Aerospace Sciences 72(2022) 3–6. doi.org/10.1016/j.paerosci.2014.09.009.

[3] R. M. Cummings, S. A. Morton. Overview of the DoD HPCMP Hypersonic Vehicle Simulation Initiative, in 22nd AIAA International Space Planes and Hypersonic Systems and Technologies Conference, AIAA Press, Orlando, FL, 2018. https://doi.org/10.2514/6.2018-5205.

[4] W. H. Yan, R. R. Xue. Comparison of turbulence models for numerical simulation of low-speed flow around NACA4412 airfoil, Acta Aeronautica Et Astronautica Sinica 38.S1 (2017) 33–40. doi:10.7527/S1000-6893.2017.721515.

[5] W. H. Yan. Steady/Unsteady Numerical Study of NACA4412 Airfoil around Flow, Science Technology and Engineering 17.02 (2017) 283-287.

[6] F. S. Qiu, W. H. Lin, C. Y. Ren. Numerical analysis of flow around the wing of light sport aircraft

based on MDR k-ε turbulent model, Journal of Shenyang Aerospace University 37.01 (2020) 1-7.

[7] Y. X. Yang, M. S. Zhao, D. C. Wan. Numerical simulation of cavitation around NACA0012 hydrofoil based on different mesh encryption methods, in Proceedings of the 31st National Conference on Hydrodynamics, JHD Press, Shanghai, 2020, pp. 947–955. doi:10.26914/c.cnkihy.2020.037552

[8] Y. Qian, H. Jiang. Dynamic Stall Simulation of NACA0012 Airfoil Based on Dynamic Grid, Computer Simulation 37.04 (2020) 44-47.

[9] H. Zhao, X. Z. Hu, J. Zhang, et al. Effects of uncertainty in turbulence model coefficients on flow over airfoil simulation, Acta Aeronautica Et Astronautica Sinica 38.S1 (2017) 33–40. doi:10.7527/S1000-6893.2018.22581.

[10] R. P. Gu, G. P. Song, W. Liu. Numerical Analysis on Aerodynamic Characteristics of the Flows with High Reynolds Number around Two-dimensional Airfoil, Science Technology and Engineering 14.21 (2014) 21671-1815.

[11] Y. L. Xue, X. L. Zhao, W J Sun. Numerical simulation of dynamic airfoil stall based on SDES method, Chinese Journal of Applied Mechanics (2022).

[12] Y. Zhang, L. Du, W. Zhang, et al. Research on data assimilation strategy of turbulent separated flow over an airfoil. Appl. Math. Mech.-Engl. Ed. 43(2022) 571–586. doi.org/10.1007/s10483-022-2827-7.

[13] N. Gregory, C. L. O'Reilly, Low-speed aerodynamic characteristics of NACA 0012 aerofoil section, including the effects of upper-surface roughness simulating hoar frost, 1970. URL: https://reports.aerade.cranfield.ac.uk/handle/1826.2/3003.

[14] W. H. Yan, T. F. Peng, Y. Yong, Numerical study of transonic separation flow using an anisotropic turbulence model, Journal of Aerospace Power 35.01 (2020) 114–125. doi:10.13224/j.cki.Jasp.2020.01.014.

[15] P. R. Spalart, S. R. Allmaras. A one-equation turbulence model for aerodynamic flows, in American Institute of Aeronautics and Astronautics 30th Aerospace Sciences Meeting and Exhibit. Reno, NV, U.S.A. 1992. doi:10.2514/6.1992-439.

[16] B. Diskin, J. L. Thomas, C. L. Rumsey, et al. Grid-Convergence of Reynolds-Averaged Navier-Stokes Solutions for Benchmark Flows in Two Dimensions, AIAA Journal 54.09(2022) 2563-2588. doi: 10.2514/1.J054555.

[17] B. Diskin, Grid Convergence for Turbulent Flows (Invited), in American Institute of Aeronautics and Astronautics 53rd AIAA Aerospace Sciences Meeting, AIAA Press, Kissimmee, Florida, 2015. doi:10.2514/6.2015-1746.